

# Emergence of spin-phonon coupling in Gd-doped $\text{Y}_2\text{CoMnO}_6$ double perovskite oxide: a combined experimental and ab-initio study

Anasua Khan<sup>1</sup>, Debdatta Banerjee<sup>2</sup>, Divya Rawat<sup>3</sup>, T.K Nath<sup>1</sup>, Ajay Soni<sup>3</sup>,  
Swastika Chatterjee<sup>2</sup>, and A.Taraphder<sup>1</sup>

<sup>1</sup>*Department of Physics, Indian Institute of Technology, Kharagpur-721302, West Bengal, India*

<sup>2</sup>*National Centre for High-Pressure Studies and Department of Earth Sciences, Indian Institute of  
Science Education and Research Kolkata, Nadia- 741246, West Bengal, India*

<sup>3</sup>*School of Physical Sciences, Indian Institute of Technology Mandi, Mandi-175005, Himachal Pradesh,  
India*

## Abstract

One of the fundamental interactions that is found in many functional materials is the spin-phonon coupling (SPC), which is at the heart of many novel functionalities. The simultaneous presence of multi-magnetic phases makes SPC even more intriguing. We have used Raman spectroscopy as well as first-principles methods to investigate the possibility of the appearance of SPC in Gd-doped  $\text{Y}_2\text{CoMnO}_6$  (YGCMO) double perovskite oxide and the influence of anti-site disorder on the same. YGCMO is found to exhibit anti-site disorder leading to both ferromagnetic (between Co and Mn) and anti-ferromagnetic interactions (Co-Co, Mn-Mn, Gd-Co/Mn). An analysis of the temperature-dependent phonon frequency for the stretching modes of YGCMO, obtained using RAMAN spectroscopy, indicates that SPC is possibly emerging from simultaneous presence of ferromagnetic and antiferromagnetic interactions. The nature of the phonon linewidth and the insulating state of the material eliminate the role of magnetostriction on the observed anomaly. The spin-phonon coupling strength comes out to

be  $0.29 \text{ cm}^{-1}$ . Our experimental findings are corroborated by first-principles DFT calculations which indicate the presence of SPC in ordered YGCMO getting enhanced in the presence of anti-site disorder. This indicates a strong influence of B-site (Co/Mn) ordering on SPC in the bulk double perovskite systems. An analysis of the cause behind the enhanced SPC in the presence of anti-site disorder is also presented.

## 1 Introduction

Multifunctional materials with correlated electronic structures have of late witnessed a surge in interest due to their inherent fundamental physics [1] (like frustrated magnetism and various spin states) and potential devices application (such as memories [2] and spintronics [3]). The strong correlation between the spin, charge, orbital, and lattice degrees of freedom is responsible for such emergent properties [4, 5]. In this regard, the compounds with the generic formula  $R_2\text{BMnO}_6$  (R=rare earth B = transition metal) have been found to hold great promise.

In general, the ordered double perovskite (DP)  $R_2\text{BMnO}_6$  materials are found to be ferromagnetic (FM) in nature by virtue of the  $\text{B}^{2+}\text{-O-Mn}^{4+}$  superexchange interaction [6, 7]. Previous experimental and theoretical research on this class of materials reports the emergence of several novel functionalities, namely, magnetocapacitance, magnetoresistance, relaxor ferroelectricity, and multiferroicity [9, 10, 11, 12]. Besides, the nature of order/disorder at the B and Mn sites in these DP materials has been found to greatly influence the electronic, magnetic, vibrational, and dielectric properties of the material [13, 14, 15, 5, 16]. It has been found that phonons as well as dielectric response of some perovskite systems in the microwave region are modified by the antisite defects [17, 18]. Additionally, the emergence of relaxor ferroelectricity in  $\text{La}_2\text{NiMnO}_6$  can be explained to a great extent by the appearance of anti-site disorder in this material [19]. Anti-site disorder (ASD) may also result in the suppression of ferromagnetism in some materials. This is because ASD induces  $\text{B}^{2+}\text{-O-B}^{2+}$  and  $\text{Mn}^{4+}\text{-O-Mn}^{4+}$  super-exchange interactions, which results in short range anti-ferromagnetic (AFM) interactions [30]. In summary, anti-site disorder in conjugation with mixed valences of transition metal ions and co-existing magnetic phases can give rise to multiple magnetic transitions at low temperature, low magnetic saturation value, and high coercivity in the DP system [30].

Recently the DPs containing smaller rare earth cations have been of great research interest as many theoretical, as well as experimental studies report the emergence of novel multiferroic properties [20] in these materials. Of particular interest is the Y-based double perovskite such as  $Y_2CoMnO_6$  (YCMO) and  $Y_2NiMnO_6$ , which have been found to exhibit polar nature in their magnetic ground state [21]. Moreover, first-principles calculations have shown that YCMO double perovskite oxides develop  $E^*$  type magnetic ordering which is the source of ferroelectricity in these materials [22, 23]. It also exhibits some interesting properties like disorder-induced exchange bias and other multiferroic properties.

In the past several studies have delved into the electronic, magnetic, optical, and transport properties of DP systems [5, 13]. It is now well-understood that the coupling of phonons with other degrees of freedom may play a vital role in dictating several properties of these systems and an investigation of the nature of the “coupling” is crucial for understanding these systems better. As a result, a qualitative model based on spin-phonon coupling was proposed earlier for YCMO [24] in order to explain magnetically induced ferroelectricity in this material. SPC is known to play a vital role in deciding the physical properties of the multiferroic systems where magnetization and electric polarization are coupled through lattice dynamics. In a strongly correlated system, the richness of the novel functionalities depends on the coupling of magnetic spins, the crystal lattice, and lattice vibrations. The interaction is complex but rich in the case of DP materials as it has two different magnetic species. SPC provides a fundamental background to understand various phenomena, such as magneto-thermal transport and magnetoelectric coupling. Spin-phonon coupling also facilitates the design of different spintronic devices with low-power and high-speed operations. For instance, external magnetic fields are used to regulate magnetic refrigeration, isothermal entropy, and adiabatic temperature. Furthermore, spin-phonon coupling helps to explain the thermal Hall Effect, relaxation time in spintronics, etc. [25]. SPC also provides a chance to modulate the functionality of transition metal oxides (TMO) [27]. Therefore, it is necessary to develop a detailed understanding of SPC in the system. Moreover, the spin-phonon coupling of DP system can be changed with lattice parameters such as cationic size, bond length and bond angle [26]. In case of DP compound in thin film, the SPC gets reduced when La is entirely replaced by Gd [28]. Again, Kumar *et al.* investigated that the SPC value gets weakened with the decrease in ionic radius of A-site cation in DP thin film [26]. This is related to the induced chemical pressure

in the system, which modifies the FM superexchange interaction due to decrease in bond length of TM ions. On the other hand, Co-based DP compound LCMO exhibits SPC in thin films, whereas phonon modes remain unaffected due to change in magnetic ordering in bulk sample [28].

In this study, we have replaced 50%  $Y^{3+}$  ions with  $Gd^{3+}$  ions to account for the effect of both local distortion and magnetism on SPC in YGCMO compound. For this purpose, temperature-dependent Raman spectroscopy along with first-principles DFT calculations are employed to investigate SPC in this DP compound [29]. It can also unveil the origin of SPC, whether it is direct or due to magnetostriction.

## 2 Experimental and Computational Details

The polycrystalline, single-phase double perovskite sample of  $Y_{1-x}Gd_xCoMnO_6$  ( $x=0.5$ ) (YGCMO) was synthesized by well known chemical sol-gel method. Initially, a stoichiometric amount of  $Y_2O_3$ ,  $Gd_2O_3$  and  $Co(NO_3)_2 \cdot 6H_2O$ ,  $Mn(CH_3COO)_2 \cdot 4H_2O$  were dissolved in diluted nitric acid and deionized water, respectively followed by the addition of citric acid to ensure the completion of the reaction. The ensuing solution was first heated at 90 °C for two hours, then finally heated at 150 °C to evaporate the solvent completely. The resultant black fluffy powder was heated at 1100 °C for ten hours with several intermediate grinding. For measurement purposes, pellets have been made and sintered at 1200 °C for 12 h.

The phase purity of the polycrystalline bulk sample was verified by the X-ray powder diffraction technique. The obtained XRD pattern and its Rietveld refinement confirmed that Gd-substituted YCMO crystallizes in monoclinic symmetry as a prime phase (99.42%) [30], reported in our previous work. X-ray Photoelectron spectroscopy measurement was performed to determine the valence states of B site cations in the YGCMO compound. The results conclude the presence of  $Co^{2+}$ ,  $Co^{3+}$ ,  $Mn^{3+}$  and  $Mn^{4+}$  ions in our sample [30]. Multimagnetic phases are observed in our sample, revealed by magnetic measurement using SQUID [30].

Raman scattering measurements were performed using Horriba Jobin Vyon LabRAM HR Evolution Raman spectrometer equipped with Czerny-turner grating (1800 gr/mm), 633 nm laser excitation of 1.25 mW power, 60s acquisition time, and Peltier cooled CCD detector. Low temperature-dependent Raman measurements were performed using a Montana cryostat in the temperature

range of 4-300 K with the temperature step 20 K. An ultra-low frequency filter was used to access low-frequency Raman modes. All the spectra were fitted by the Lorentzian function to evaluate the phonon frequency of the Raman modes.

All theoretical calculations have been performed using first principles density functional theory (DFT) [31, 32] using projector augmented wave method (PAW) [33, 34] as implemented in the VASP code [35, 36]. The Perdew-Burke-Ernzerhof (PBE) [37] formalism of the generalized gradient approximation (GGA) has been used as the exchange correlation functional in our calculations. An energy cut-off of 550 eV and kpoint mesh of  $6 \times 6 \times 6$  was applied using the Monkhorst-Pack method [38]. The energy convergence with respect to all computational parameters was ascertained. A complete optimization of the crystal structure was performed till the forces were less than 0.001 eV/Å. In order to take into account, the missing correlation beyond GGA, a supplemented GGA+U calculation was performed with the U-J (U: on-site Coulomb repulsion; J: Hunds coupling strength) [39] value as 3 eV for Co-d, 3 eV for Mn-d [13] and 6 eV for Gd-f-orbitals [30]. Phonon frequencies and eigen vectors were determined from the dynamical matrices which were in turn determined from the force constants obtained using density functional perturbation theory (DFPT) [40] as implemented in VASP and post-processed using PHONOPY [41].

### 3 Results and discussion

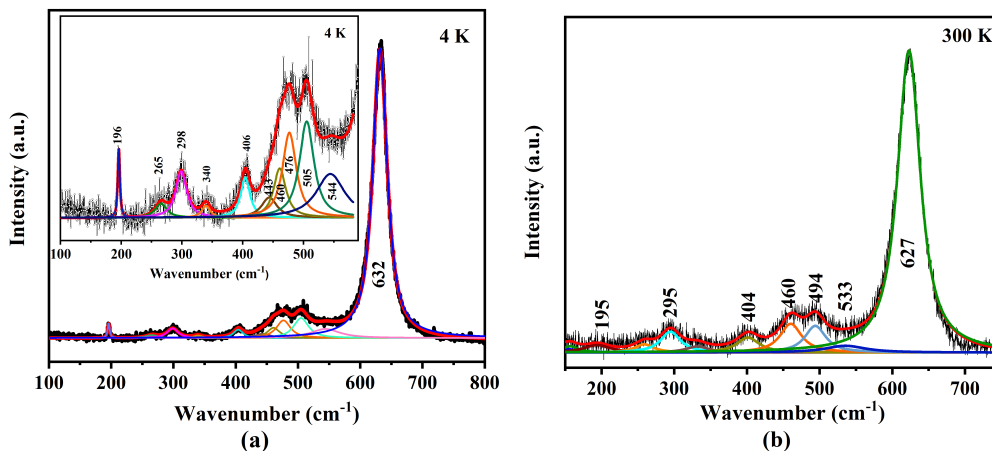


Figure 1: Temperature dependent Raman spectra of Gd-doped YCMO at (a) 4 K and (b) 300 K. The inset shows low wavenumber region. The red solid line shows the net fitted spectrum.

The irreducible representation of the possible Raman modes of Gd-substituted YCMO at  $T=4$

K and 300 K are shown in Fig. 1(a) and (b), respectively. The absence of most intense Raman peak of  $\text{Y}_2\text{O}_3$  near  $377\text{ cm}^{-1}$  [42, 43] indicates the absence of a secondary phase ( $\text{RE}_2\text{O}_3$ ) [44] in the system. Fig. 1(a) depicts eleven first-order Raman modes resolved at  $T=4\text{ K}$ , and their frequencies are determined by deconvoluting the spectrum with the Lorentzian line profile. However, only seven Raman modes are deconvoluted at room temperature. No structural phase transition is observed throughout the temperature variation, confirming that the YGCMO remains in a monoclinic structure with space group  $P2_1/n$ , shown in Fig. 2 (a), (b), and (c). In this symmetry,  $4e$  sites are generally occupied by the rare earth ions and Oxygen atoms, whereas Co and Mn ions prefer  $2c$  and  $2b$  sites, respectively. The schematic of the structure is shown in Fig. 6.

The low symmetry structures of double perovskites result from a distorted cubic  $\text{Fm}\bar{3}\text{m}$  aristotype lattice [45]. From the group theory calculation, 24 Raman active modes are expected to be observed for this space group, and its distribution according to the irreducible representation of  $2/m$  factor point group is given as follows:  $6T(3A_g + 3B_g) + 6L(3A_g + 3B_g) + 2\nu_1(A_g + B_g) + 4\nu_2(2A_g + 2B_g) + 6\nu_5(3A_g + 3B_g)$ , which can be written as  $12A_g + 12B_g$  [29]. Lattice modes ( $T$ = translational and  $L$ = librational) are observed below  $380\text{ cm}^{-1}$  whereas internal modes corresponding to oxygen octahedron ( $\nu_1, \nu_2$ , and  $\nu_5$ ) are detected above  $380\text{ cm}^{-1}$  [29]. Generally, vibrational modes correspond to oxygen atoms connected with higher valence ions [46]. In this experiment, out of 24 Raman active modes, 11 Raman modes can be resolved at  $T=4\text{ K}$  which is notably larger than the resolved mode for other La-based double perovskites [15, 29]. Smaller ionic radii of  $\text{Y}^{3+}$  and  $\text{Gd}^{3+}$  cation ( $r = 1.20\text{ \AA}$  and  $r = 1.22\text{ \AA}$ ) in YGCMO lead to more distortion in the structure, which results in major octahedra tilts. As a consequence, a significant number of modes have been observed. In comparison with LCMO, the Raman bands split more for YGCMO due to strong monoclinic distortion [47].

In the past, Iliev *et al.* [29] have identified the Raman modes for Mn-based DP system from the semiempirical calculation, and it is in good agreement with their experimental results. Therefore, based on some of the previous works [29, 48], Raman modes at  $632\text{ cm}^{-1}$ ,  $505\text{ cm}^{-1}$ ,  $340\text{ cm}^{-1}$ ,  $298\text{ cm}^{-1}$ ,  $265\text{ cm}^{-1}$ , and  $196\text{ cm}^{-1}$  observed in our experiment can be assigned to  $A_g$  symmetry and also known as stretching mode (S). Here Co/Mn-O bond involves both in-plane and out-of-plane vibrations and those detected at  $544\text{ cm}^{-1}$ ,  $476\text{ cm}^{-1}$ , and  $406\text{ cm}^{-1}$  have  $B_g$  symmetry and are also known as anti-stretching mode (AS). Here  $\text{O}^{2-}$  ions vibrate perpendicularly to the Co/Mn-O bond.

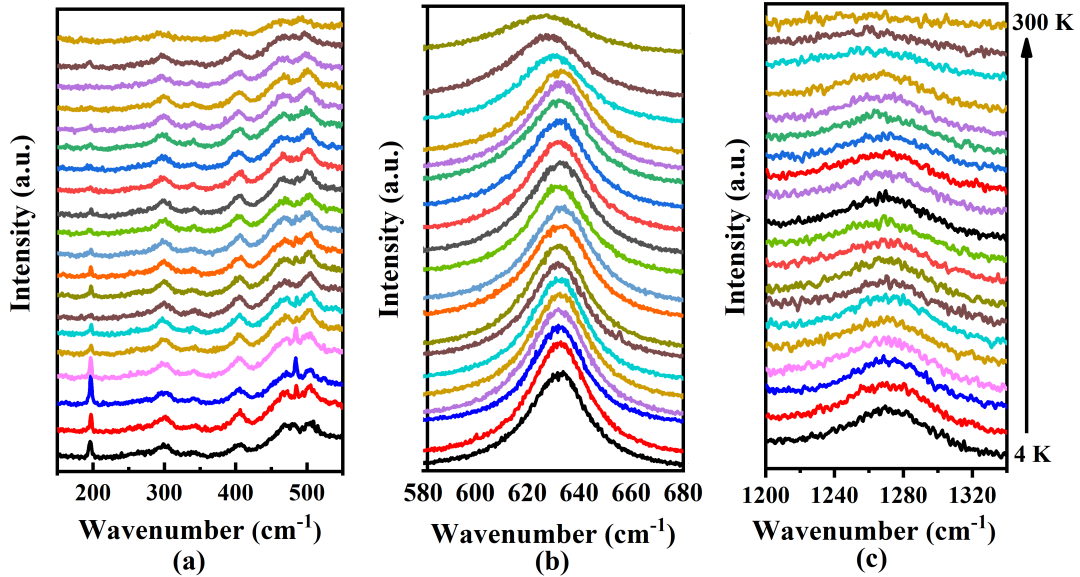


Figure 2: Temperature-dependent Raman spectra of Gd-doped YCMO in the (a) low wavenumber region, (b) main vibrational mode, and (c) high wavenumber region.

The mode noticed at higher wave number  $1270 \text{ cm}^{-1}$  corresponds to the second-order overtone of breathing mode [49].

In order to study spin-phonon coupling in our sample, the effect of temperature on the phonon modes has been analyzed. The recorded temperature dependence of the Raman spectrum between 4 K and room temperature is shown in Fig. 2 (a), (b), and (c). These figures illustrate the impact of magnetic ordering on the lattice vibration. Generally, in manganite perovskite, the stretching mode shows spin-phonon coupling [50]. In our study, the temperature dependence of two of the most representative Raman modes are presented in Fig. 3 (a-b). Temperature dependence of phonon frequency due to anharmonic contribution (due to lattice contraction) proposed by Balkanski [51] can be written as follows,

$$\omega(T) = \omega(0) - C \left( 1 + \frac{2}{e^{\frac{\hbar\omega_0}{kT}} - 1} \right) \quad (1)$$

where  $C$  (anharmonic constant) and  $\omega_0$  (position of the Raman mode at the temperature  $T=0$  K) are the adjustable parameters. In the absence of any phase transition, temperature-dependent Raman mode should follow the above anharmonic relation. It is seen that the most intense Raman mode, also known as stretching mode (observed at  $632 \text{ cm}^{-1}$ ), fits nicely with the anharmonic model above  $T_C$ , shown in Fig. 3(a). This mode shows a deviation from the above model for  $T \leq T_C$  with two distinct discontinuities at  $T_C$  and  $T_N$ , respectively. The deviation is more pronounced

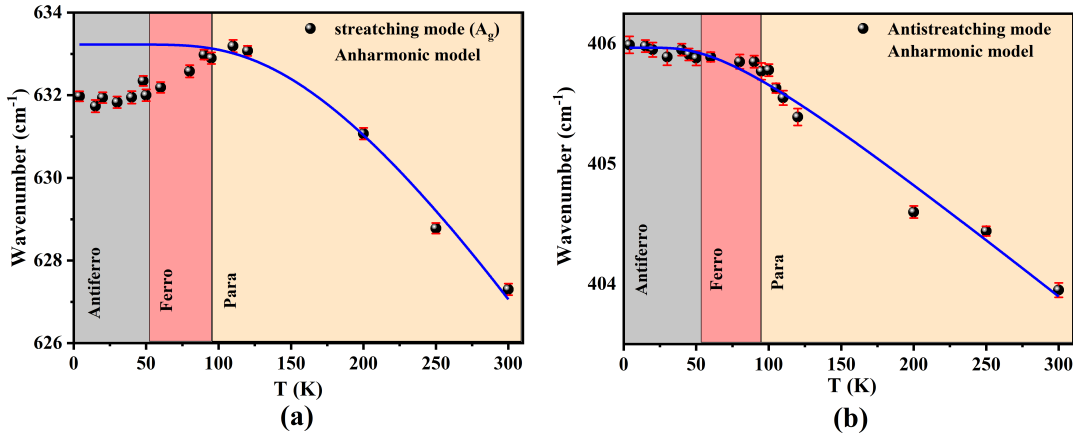


Figure 3: Temperature-dependence of phonon positions of (a)  $A_g$  stretching mode, (b)  $B_g$  anti-stretching mode for YGCMO (black sphere). The blue line represents the approximation from the above anharmonic model. The error bars are the standard deviation of the peak positions as obtained from the fitting procedure.

with lowering the temperature. This anomalous behavior could arise due to the renormalization of phonons induced by the ferromagnetic ordering of Co-Mn ions and results in the coupling between spin and lattice (phonon) degrees of freedom [52]. A similar feature is observed in several double perovskite manganite systems [53, 54]. On the other hand, the AS Raman mode observed at  $406 \text{ cm}^{-1}$ , fits well with the above anharmonic model throughout the investigated temperature range except near  $T_C$ . At lower temperatures, the phonon frequencies become nearly constant for this mode. This temperature-independent behavior of phonon frequencies at lower temperatures could happen due to a change in magnetic spin structure or weak ferromagnetic ordering [55]. Our previous study shows that below  $T_{Cd}$  (Gd ordering temperature), Gd spins are at  $ab$  plane, which was in  $c$  direction [30].

The temperature dependence of linewidth of stretching and anti-stretching modes are plotted in Fig. 4 (a-b) to investigate the role of magnetostriction in this coupling. Raman linewidth is associated with phonon life-time that is not affected by lattice volume changes i.e. magnetostriction effect. Generally, at higher temperatures, a significant anharmonic effect has been observed due to rigorous atomic vibration of the atoms about their mean position. However, this anharmonic effect gets reduced with a decrease in temperature due to reduced phonon-phonon interactions. As a result, phonon-lifetime increases or FWHM decreases. We observed that both the curves show anomaly upon entering into the magnetic region with the discontinuities at  $95.5 \text{ K}$  ( $T_C$ ) and  $47 \text{ K}$  ( $T_N$ ), respectively, which suggests relative dependence of phonon lifetime with magnetic ordering.



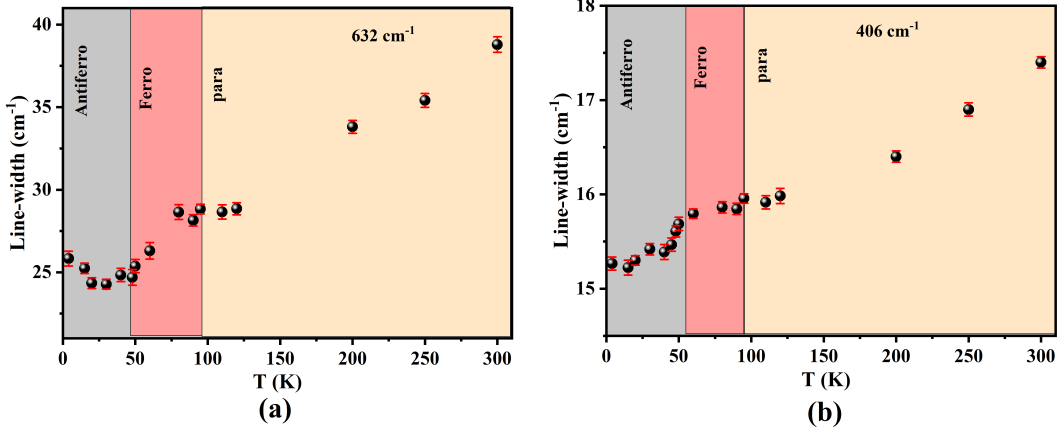


Figure 4: Temperature-dependence of Raman line width (FWHM) of (a)  $A_g$  mode, and (b)  $B_g$  mode. The error bars are the standard deviation of the peak positions as obtained from the fitting procedure.

Therefore, strong interaction between phonon and magnetic degree of freedom leads to an increase in linewidth at lower temperatures i.e., a decrease in phonon lifetime. Usually, the linewidth is affected by spin-phonon coupling and electron-phonon coupling [61]. The total electronic density of states for YGCMO shows that it is insulating in nature( refer to Fig.S2 in SI). Therefore, the anomaly in linewidth with temperature is ascribed to spin-phonon coupling [61].

The detailed structural and magnetic study on YGCMO has been done in our previous paper [30] which reveals that the compound is partially disordered with  $\text{Co}^{2+}$ ,  $\text{Co}^{3+}$ ,  $\text{Mn}^{3+}$  and  $\text{Mn}^{4+}$  ions. An appreciable amount (38%) of antisite disorder is found in this sample. It exhibits three different magnetic transitions: i) FM transition triggers at  $T_C=95.5$  K due to  $\text{Co}^{2+}$ -O- $\text{Mn}^{4+}$  superexchange interaction. ii) Antiferromagnetic (AFM) transition occurs at  $T_N=47$  K due to  $3d-4f$  exchange interaction of Co/Mn and Gd sublattices and ASD disorder present in the sample. iii) At  $T \leq 20$  K,  $\text{Gd}^{3+}$ -O- $\text{Gd}^{3+}$  interactions become active and give rise to AFM interactions. More details are found in SI (refer to Fig.S1).

The careful observation of the above temperature-dependent frequency and linewidth plot reveals a new phonon renormalization arising at  $T_N$  due to AFM ordering of Gd-Co/Mn spins, implying the presence of spin-phonon coupling. This result suggests that the FM phase i.e. ordered regions and similar disordered clusters exist together in this sample, where predominate AFM interactions produced from  $\text{Co}^{3+}$ -O-  $\text{Co}^{3+}$ ,  $\text{Mn}^{3+}$ -O- $\text{Mn}^{3+}$ ,  $\text{Co}^{2+}$ -O-  $\text{Co}^{2+}$ ,  $\text{Mn}^{4+}$ -O- $\text{Mn}^{4+}$ , and  $3d-4f$  exchange pathways. Besides magnetic measurements, Raman spectroscopy is a powerful tool to detect magnetic inhomogeneity present in the sample.

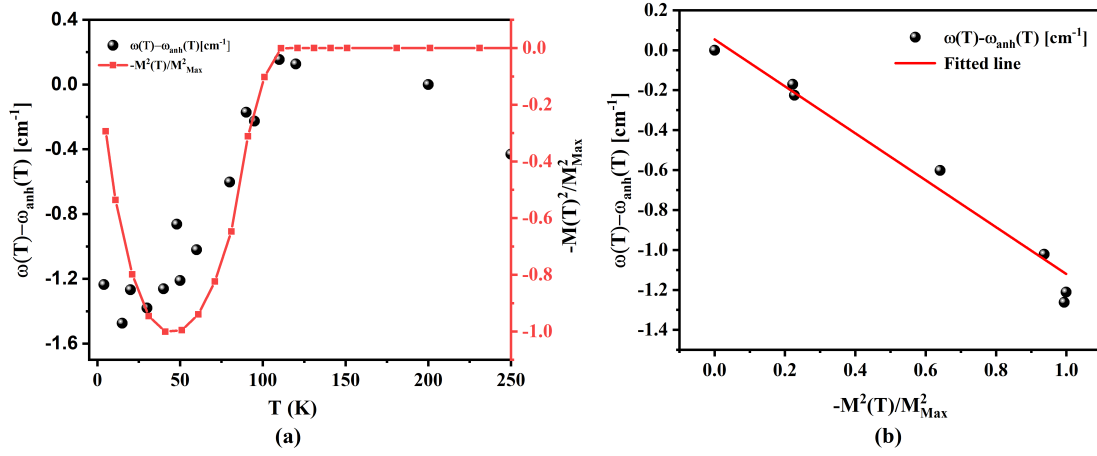


Figure 5: (a) A comparison of the deviation ( $\Delta\omega(T)$ ) of  $A_g$  stretching mode from the anharmonic model and the normalized magnetization  $\frac{M^2(T)}{M_{max}^2}$ . (b) the corresponding linear dependence of  $\Delta\omega(T)$  on the squared relative magnetisation  $\frac{M^2(T)}{M_{max}^2}$ .

To get detailed insight into the anomalous behavior of Raman modes, the renormalization of phonon frequency with normalized magnetic moment has been plotted in Fig. 5(a). Usually, the deviation of phonon mode from the anharmonic model can be explained by the spin-spin correlation function in magnetic oxides [28].

$$\Delta\omega_{SPC}(T) = \omega(T) - \omega_{anh}(T) \approx -\lambda\langle\mathbf{S}_i \cdot \mathbf{S}_j\rangle \quad (2)$$

where  $\omega(T)$  is the normalized phonon frequency due to SPC,  $\omega_{anh}$  is the phonon frequency in the absence of SPC,  $S_i$  and  $S_j$  are nearest neighbor spins at  $i^{th}$  and  $j^{th}$  sites, respectively.  $\lambda$  denotes the strength of spin-phonon coupling.  $\Delta\omega$  is obtained by taking the difference between calculated and observed phonon frequencies. According to mean-field theory, the spin-spin correlation function can be connected to magnetization by the equation  $\Delta\omega_{SPC} \approx (M(T)/M_{max})^2$ , where  $M(T)$  and  $M_{max}$  are the magnetization at  $T$  and saturation magnetization approximated to  $T=0$  K, respectively. Therefore, by considering the four nearest neighbors for each B site cation,  $\Delta\omega_{SPC}$  can be written as follows [58]:

$$\Delta\omega_{SPC} \approx -\lambda\langle\mathbf{S}_i \cdot \mathbf{S}_j\rangle \approx -4\lambda\frac{M^2(T)}{M_{max}^2} \quad (3)$$

The spin-phonon coupling constant value  $\lambda$  is estimated by using the above approach. Its value can be positive or negative depending upon phonon hardening or softening. In Fig. 5(a), it is seen that there is a good overlap of both  $\Delta\omega_{SPC}$  and normalized magnetization  $\frac{M^2(T)}{M_{max}^2}$  up to 95 K, after that

a deviation in the magnitude of  $\Delta\omega_{SPC}$  occurs. It signifies that the origin of anomalous softening is ascribed to spin-phonon coupling. The occurrence of this unconventional behavior might be caused by competition between FM and AFM interactions due to ASD present in the sample. ASD occurs in DP compounds very often because of small charge differences and ionic radii differences of the TM ions. As stated above, our sample contains 38% ASD, which helps to originate different types of AFM ( $\text{Co}^{2+}\text{-O-Co}^{2+}$ ,  $\text{Mn}^{4+}\text{-O-Mn}^{4+}$ , etc.) along with FM ( $\text{Co}^{2+}\text{-O-Mn}^{4+}$ ) interactions, leading to magnetic frustration in the systems. In our sample, another source of AFM is the interaction between Co/Mn and Gd sublattices. Therefore, different values of magnetic coupling  $J_{ij}$  can contribute in different ways to the phonon renormalization induced by magnetic ordering. It makes the spin-phonon coupling more complex and causes deviation from mean field approximation. A similar kind of deviation is observed in  $\text{La}_2\text{CoMnO}_6$  [57],  $\text{Gd}_2\text{CoMnO}_6$  [58], and  $\text{Lu}_2\text{CoMnO}_6$  [59], where FM and AFM interactions coexist together.

Spin-phonon coupling strength ( $\lambda$ ) is determined by taking a quarter of the slope of the linear relationship of  $\Delta\omega_{SPC}$  vs.  $\frac{M^2}{M_{max}^2}$  [26] shown in Fig. 5 (b). The value is found to be  $0.29 \text{ cm}^{-1}$ . It has been observed that SPC value is always lower for bulk DP than thin film [28]. Silva *et al.* reveal that ordered bulk LCMO does not show SPC whereas disordered GCMO exhibits SPC to a greater extent [62]. Again, Meyer *et al.* [28] show that spin-phonon coupling coefficient value is lower for disordered LCMO in thin film than the ordered one. Thus B-site cationic ordering has not only influenced the magnetic properties of YGCMO perovskite significantly but also affects its phonon properties and spin-phonon coupling strength  $\lambda$  to a great extent.

SPC in the YGCMO compound is further investigated by first-principle calculations. We have

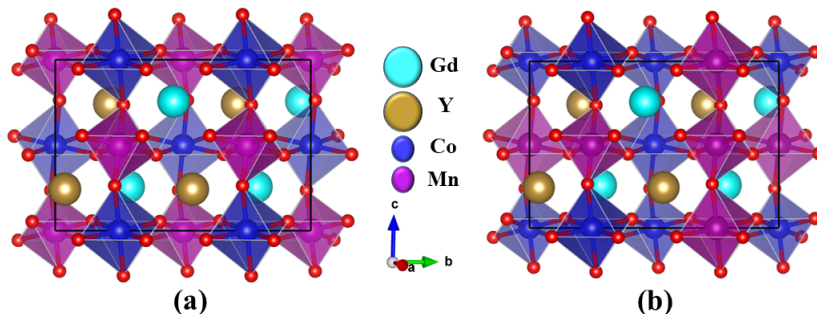


Figure 6: Lowest energy crystal structure of (a) ordered YGCMO and (b) disordered YGCMO. The blue and purple balls represent Co and Mn atoms respectively, and sit at the centre of the octahedra. Here Y and Gd atoms are represented by golden and cyan big balls, sitting in the cage formed by  $\text{CoO}_6$  and  $\text{MnO}_6$  octahedra.

considered a supercell of size  $1 \times 2 \times 1$  containing 40 atoms i.e, there are 4 Y, 4 Gd, 4 Co, 4 Mn, and 24 O atoms in each supercell. The structure was fully optimized, starting from the room temperature experimental data. Fig. 6(a) shows the lowest energy ordered structure of YGCMO where Co and Mn octahedra are arranged alternately. To determine the influence of anti-site disorder on the nature of SPC, starting from the ordered  $1 \times 2 \times 1$  crystal structure, we have manually introduced some anti-site disorder. This disordered structure thereafter underwent a complete optimization (see Fig. 6 (b)). The total electronic density of states for the disordered structure (which contains Co-Co, Co-Mn, and Mn-Mn interactions) shows that the sample is insulating with a band gap of 1 eV (refer to Figure S2 of the SI). To determine the magnetic ground state, we have performed total

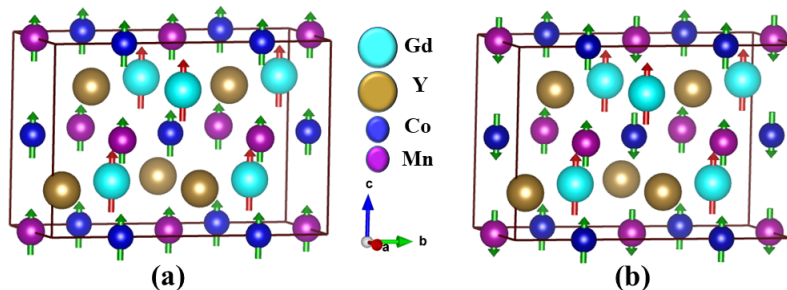


Figure 7: Energetically preferred spin configurations of ordered YGCMO (a) Ferromagnetic ordering; (b) C-type AFM ordering. Here, blue, and purple small balls and golden and cyan big balls represent Co, Mn, Y, and Gd atoms respectively. The red arrows denote the spins on Gd atoms and green arrows represent the spins on Co and Mn atoms.

energy calculations on the ferromagnetic, C-, G-, and A-type antiferromagnetic and ferrimagnetic configurations of ordered-YGCMO. These magnetic interactions were considered among the Co and Mn ions, whereas the Gd moments were made to orient along the z-direction in all the calculations. Our calculations indicate that the ferromagnetic state (see Fig. 7(a)) has the lowest energy followed by the C-type AFM magnetic configuration (see Fig. 7 Y(b)). The relative energies of the different magnetic orderings with respect to the ferromagnetic state have been tabulated in Table 1. To

Table 1: **Total energy of different magnetic configurations of ordered YGCMO with respect to the ferromagnetic state.**

Spin configurations	Relative energy values (eV/f.u.)
FM	0.0
C-type AFM	0.214
G-type AFM	0.259
A-type AFM	1.863
Ferrimagnetic	0.252

investigate whether there is a coupling between the spin and the lattice degrees of freedom, we have calculated the total phonon density of states for the two lowest energy magnetic configurations, namely, the ferromagnetic and the C-type antiferromagnetic state, in both its ordered and anti-site disordered state (as shown in Fig. 6). The total phonon density of states for these two configurations

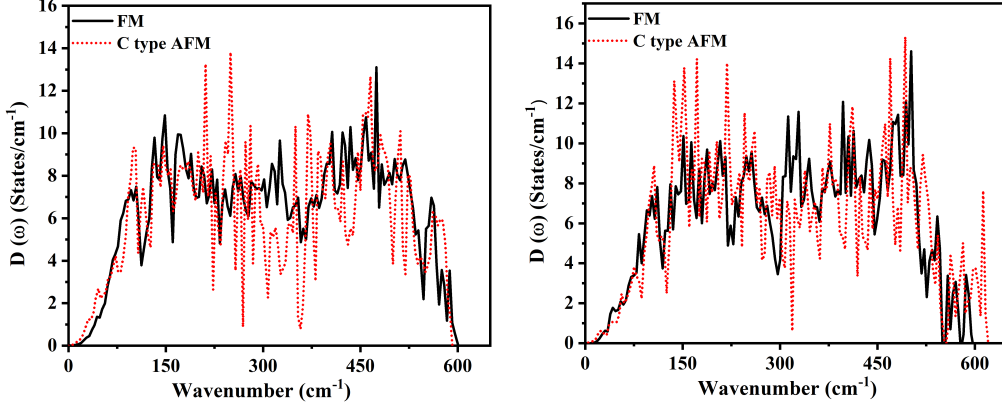


Figure 8: Comparative total phonon density of states of FM and C-type AFM for (a) ordered state, (b) disordered state.

Table 2: The average bond angles between transition metal elements obtained from DFT calculations are as follows

	Co-O-Mn ( $^{\circ}$ )	Co-O-Co ( $^{\circ}$ )	Mn-O-Mn ( $^{\circ}$ )
FM-ordered	144.85	-	-
C-type AFM-ordered	145.31	-	-
FM-disordered	146.66	147.28	145.16
C-type AFM disordered	144.78	145.09	144.82

is shown in Fig. 8. The absence of imaginary modes affirms the dynamical stability of both the magnetic configurations. It is evident from Fig. 8(a) that with the change in magnetic ordering, there is an alteration in the phonon density of states, indicating that spin-phonon coupling is active in this system. The partial phonon density of states for FM and C-type magnetic configuration is presented in Figure S3 of the SI. We have also checked the influence of disorder at Co and Mn on the spin-phonon coupling, as presented in Fig. 8(b). Our calculations indicate that with the introduction of disorder in the system, the shift between prominent modes further increases by about  $\approx 3\%$ . To investigate the cause behind the enhanced spin-phonon coupling in the case of disordered YGCMO, we performed a detailed structural analysis of the sample in the presence/absence of disorder. It was observed that in the ordered sample the Co-O-Mn bond angle was enhanced by  $0.46^{\circ}$  as the

Table 3: The average bond length of Co-O and Mn-O obtained from DFT are as follows

	Co-O (Å)	Std. deviation (Å)	Mn-O (Å)	Std. deviation (Å)
FM-ordered	2.0809	0.00	1.9444	0.00
C-type AFM-ordered	2.0926	0.0011	1.9400	0.0006
FM-disordered	2.0426	0.05537	1.9731	0.02856
C-type AFM disordered	2.0447	0.05997	1.9567	0.04715

magnetic configuration was changed from FM to C-type. However, the same was found to be reduced by  $1.88^\circ$  for the disordered sample (refer to Table 2). Analysis of the bond lengths of the  $\text{CoO}_6$  and  $\text{MnO}_6$  octahedra showed that in ordered YGCMO the average Co-O bond length is found to increase by  $0.0117 \text{ \AA}$  and the average Mn-O bond length was found to decrease by  $0.0044 \text{ \AA}$  as the magnetic configuration was changed from FM to C-type AFM. On the contrary, for similar magnetic transformations, both the average Co-O and Mn-O bond lengths were found to get enhanced and reduced by  $0.0021 \text{ \AA}$  and  $0.0164 \text{ \AA}$ , respectively. However, there is in general an increase in the distortion of the  $\text{CoO}_6$  and  $\text{MnO}_6$  octahedra with change in magnetic ordering, which is found to increase with the introduction of anti-site disorder. It has been observed previously [63] that the dependence of the Raman modes on the bond length ( $l$ ) is by  $1/\sqrt{l}$ . Therefore, the modulation in bond length of a specific atom engaged with a particular vibration can lead to shifts in mode positions. This is also evident in our first-principles calculations which show that in the presence of anti-site disorder, the magnetism induced distortion of the lattice is more which eventually gets reflected in the phonon spectra.

## 4 Conclusion

In summary, temperature-dependent Raman spectroscopy and first-principles methods have been used for investigating the spin-phonon coupling of Gd-substitute YCMO. No remarkable spectral changes throughout the investigating temperature range confirm that the sample holds its  $P2_1/n$  symmetry. The existence of ASD within this system leads to the emergence of Ferromagnetic (Co-Mn) and Antiferromagnetic (Co-Co, Mn-Mn, Gd-Co/Mn) interactions. Anomalous softening of  $A_g$  stretching mode implies the appearance of SPC due to the presence of both FM and AFM interactions. The temperature dependence of linewidth curves of  $A_g$  and  $B_g$  modes exhibit anomalies in the ferromagnetic ( $T_c$ ) as well as the antiferromagnetic ( $T_N$ ) region. This result suggests that

there is a phonon-mediated interaction between Gd and Co/Mn spins. Again, the nature of phonon linewidth curves and the insulating nature of the material discards the effect of magnetostriction on the observed softening of  $A_g$  mode. On the other hand, phonon renormalization of  $A_g$  mode exhibits an unconventional behavior because of competing FM and AFM magnetic ordering, which is driven by ASD. The calculated value of the SPC strength is found to be  $0.29 \text{ cm}^{-1}$ . Our DFT calculations also exhibit the presence of SPC in this compound in its ordered and disordered state. Interestingly, it is observed that disordered system helps to improve the SPC value. Thus B-site ordering plays a pivotal role in SPC in the bulk YGCMO.

## 5 Acknowledgments

AK acknowledges the University Grants Commission (UGC) and the Ministry of Education (MoE) for their financial support. AK, AT, and TKN also acknowledge the National Supercomputing Mission (NSM) for providing computing resources of PARAM Shakti at IIT Kharagpur, which is implemented by C-DAC and supported by the Ministry of Electronics and Information Technology (MeitY) and Department of Science and Technology (DST), Government of India. AS would like to thank the IIT Mandi for research facilities. DB acknowledges funding from the Prime Minister's Research Fellowship scheme (PMRF) and computing facilities of IISER Kolkata. SC acknowledges funding through the IISER Kolkata start-up grant and SERB-POWER Grant (Grant No.: SPG/2021/003842).

## References

- [1] W. Eerenstein, N. D. Mathur, and J. F. Scott, *Nature (London)* **442**, 759 (2006).
- [2] J. F. Scott, *Nat. Mater.* **6**, 256 (2007).
- [3] I. Zutic, J. Fabian, and S. D. Sarma, *Rev. Mod. Phys.* **76**, 323 (2004).
- [4] J. K. Murthy, K. D. Chandrasekhar, H. C. Wu, H. D. Yang, J. Y. Lin, and A. Venimadhav, *Journal of Physics: Condensed Matter* **28**, 086003 (2016).
- [5] R. I. Dass and J. B. Goodenough, *Phys. Rev. B* **67**, 014401 (2003).

- [6] R.J. Booth, R. Fillman, H. Whitaker, A. Nag, R.M. Tiwari, K.V. Ramanujachary, J. Gopalakrishnan and S.E. Lofland. *Mater. Res. Bull.* **44**, 1559–64 (2009).
- [7] J.B. Goodenough. *Phys. Rev.* **100**, 564 (1955).
- [8] N.S. Rogado, J. Li, A.W. Sleight, M.A. Subramanian, *Adv. Mater.* **17**, 2225–2227 (2005).
- [9] K.D. Chandrasekhar, A.K. Das, A. Venimadhav, *J. Phys. Condens. Matter.* **24**, 376003 (2012).
- [10] P.R. Mandal, A. Khan, T.K. Nath, *J. Appl. Phys.* **128**, 024104 (2020).
- [11] I. Álvarez-Serrano, M.L. López, F. Rubio, M. García-Hernández, G.J. Cuello, C. Pico, M. Luisa Veiga, *J. Mater. Chem.* **22**, 11826 (2012).
- [12] M.G. Masud, A. Ghosh, J. Sannigrahi, B.K. Chaudhuri, *J. Phys. Condens. Matter.* **24**, 295902 (2012).
- [13] A. Khan, S. Chatterjee, T.K. Nath and A. Taraphder, *Phys. Rev. B* **104** 035152 (2021).
- [14] R.X. Silva, A.S. Menezes, R.M. Almeida, R.L. Moreira, R. Paniago, X. Marti, H. Reichlova, M. Mary, M. Vinicius, S. Rezende, C.W.A. Paschoal, *J. Alloys Compd.* **661**, 541–552 (2016).
- [15] K.D. Truong, J. Laverdière, M.P. Singh, S. Jandl, P. Fournier, *Phys. Rev. B.* **76** (2007) 132413.
- [16] A.J. Barón-González, C. Frontera, J.L. García-Muñoz, B. Rivas-Murias, J. Blasco, *J. Phys. Condens. Matter.* **23**, 496003 (2011).
- [17] A. Dias, L.A. Khalam, M.T. Sebastian, C. William, C.W.A. Paschoal, R.L. Moreira, *Chem. Mater.* **18**, 214–220 (2006).
- [18] A. Dias, R.L. Moreira, *J. Appl. Phys.* **94**, 3414 (2003).
- [19] M.G. Masud, A. Ghosh, J. Sannigrahi, B.K. Chaudhuri, *J. Phys. Condens. Matter* **24**, 295902 (2012),
- [20] I. O. Troyanchuk, D. D. Khalyavin, J. W. Lynn, R. W. Erwin, Q. Huang, H. Szymczak, R. Szymczak and M. J. Baran. *Appl. Phys.* **88**, 360 (2000).



- [21] M. H. Tang, Y. G. Xiao, B. Jiang, J. W. Hou, J. C. Li, and J. He, Appl. Phys. A **105**, 679 (2011).
- [22] S. Kumar, G. Giovannetti, J van den Brink and S. Picozzi , Phys. Rev. B **82** 134429 (2010).
- [23] S. Picozzi , Kunihiro Yamauchi, Ivan A Sergienko, Cengiz Sen, Biplab Sanyal, Elbio Dagotto. J. Phys.: Condens. Matter **20**, 434208 (2008).
- [24] G. Sharma, J. Saha, S.D. Kaushik, V. Siruguri, S. Patnaik, Appl. Phys. Lett. **103**, 012903 (2013).
- [25] X. Moya & N.D. Mathur. Nat. Mater. **16**, 784–785 (2017).
- [26] D. Kumar, S. Kumar and V. G. Sathe, Solid State Commun. **194**, 59 (2014).
- [27] R. Ramesh & N.A. Spaldin. Nat. Mater. **6**, 21–29 (2007).
- [28] Ch. Meyer, V. Roddatis, P. Ksoll, B. Damaschke, and V. Moshnyaga Phys. Rev. B **98**, 134433 (2018).
- [29] M. Iliev, M. Abrashev, A. Litvinchuk, V. Hadjiev, H. Guo, and A. Gupta, Phys. Rev. B **75**, 104118 (2007).
- [30] A. Khan, S. Rajput, M. Anas, V. K. Malik, T. Maitra, T. K. Nath and A. Taraphder. J. Phys.: Condens. Matter **34** 435801 (2022).
- [31] P. Hohenberg, W. Kohn. Phys. Rev. **136**, B864 (1964).
- [32] W. Kohn, L.J. Sham. Phys. Rev. **140**, A1133 (1965).
- [33] P.E. Blöchl. Phys. Rev. B **50**, 17953 (1994).
- [34] G. Kresse, D. Joubert. Phys. Rev. B **59**, 1758 (1999).
- [35] G. Kresse, J. Hafner. Phys. Rev. B **47**, 558(R) (1993).
- [36] G. Kresse, J. Furthmüller. Phys. Rev. B **54**, 11169 (1996).
- [37] J.P. Perdew, K. Burke, M. Ernzerhof. Phys. Rev. Lett. **77**, 3865 (1996).

- [38] H.J. Monkhorst and J.D. Pack Physical Review B, 13, 5188–5192 (1976).
- [39] S.L. Dudarev, G.A. Botton, S.Y. Savrasov; C.J. Humphreys; A.P. Sutton. Phys. Rev. B **57**, 1505(1998).
- [40] S. Baroni, S.D. Gironcoli, A.D. Corso, P. Giannozzi. Rev. Mod. Phys. **73**, 515 (2001).
- [41] Togo, Atsushi and Isao Tanaka. Scripta Materialia, **108**:1–5 (2015).
- [42] Y. Repelin, C. Proust, E. Husson, and J. Beny, J. Solid State Chem. **118**, 163 (1995).
- [43] B. Allieri, L. E. Depero, A. Marino, L. Sangaletti, L. Caporaso, A. Speghini, and M. Bettinelli, Mater. Chem. Phys. **66**, 164 (2000).
- [44] H. S. Nair, D. Swain, H. N. S. Adiga, C. Narayana, and S. Elizabeth, J. Appl. Phys. **110**, 123919 (2011)
- [45] M. Iliev, M. Abrashev, A. Litvinchuk, V. Hadjiev, H. Guo, A. Gupta, Phys. Rev. B **75**, 104118 (2007).
- [46] A. P. Ayala, I. Guedes, E. N. Silva, M. S. Augsburger, M. del C. Viola, and J. C. Pedregosa, J. Appl. Phys. **101**, 123511 (2007).
- [47] C. L. Bull, D. Gleeson, and K. S. Knight, J. Phys.: Condens. Matter **15**, 4927 (2003).
- [48] M. N. Iliev, M. M. Gospodinov, M. P. Singh, J. Meen, K. D. Truong, P. Fournier, and S. Jandl, J. Appl. Phys. **106**, 023515 (2009).
- [49] C. Meyer, S. Hühn, M. Jungbauer, S. Merten, B. Damaschke, K. Samwer, and V. Moshnyaga, J. Raman Spectrosc. **48**, 46 (2017).
- [50] R.B. Macedo Filho, A. Pedro Ayala, C. William de Araujo Paschoal, Appl. Phys. Lett. **102**, 192902 (2013).
- [51] M. Balkanski, R.F. Wallis, E. Haro, Phys. Rev. B. **28**, 1928–1934 (1983).
- [52] K.D. Truong, M.P. Singh, S. Jandl, P. Fournier, J. Phys. Condens. Matter. **23**, 052202 (2011).

- [53] H.S. Nair, D. Swain, H.N.S. Adiga, C. Narayana, S. Elizabeth, *J. Appl. Phys.* **110**, 123919 (2011),
- [54] R.B. Macedo Filho, A. Pedro Ayala, C. William de Araujo Paschoal, *Appl. Phys. Lett.* **102**, 192902 (2013),
- [55] Kaustuv Manna, R. Sarkar, S. Fuchs, Y. A. Onykiienko, A. K. Bera, G. Aslan Cansever, S. Kamusella, A. Maljuk, C. G. F. Blum, L. T. Corredor, A. U. B. Wolter, S. M. Yusuf, M. Frontzek, L. Keller, M. Iakovleva, E. Vavilova, H.-J. Grafe, V. Kataev, H.-H. Klauss, D. S. Inosov, S. Wurmehl, and B. Büchner, *Phys. Rev. B* **94**, 144437 (2016).
- [56] M. N. Iliev, M. V. Abrashev, A. P. Litvinchuk, V. G. Hadjiev, H. Guo, and A. Gupta, *Phys. Rev. B* **75**, 104118 (2007).
- [57] J.K. Murthy, K.D. Chandrasekhar, S. Murugavel, A. Venimadhav, *J. Mater. Chem. C* **3**, 836e843 (2015),
- [58] X.L. Wang, J. Horvat, H.K. Liu, A.H. Li, S.X. Dou, Spin glass state in Gd<sub>2</sub>CoMnO<sub>6</sub> perovskite manganite, *Solid State Commun.* **118**, 27e30 (2001).
- [59] S. Yanez-Vilar, E.D. Mun, V.S. Zapf, B.G. Ueland, J.S. Gardner, J.D. Thompson, et al., *Phys. Rev. B* **84**, 134427 (2011),
- [60] D. Kumar, S. Kumar, and V. G. Sathe, *Solid State Commun.* **59**, 194 (2014).
- [61] Venkata Srinu Bhadrani, B. Rajeswaran, A. Sundaresan and Chandrabhas Narayana . *EPL* **101**, 17008 (2013).
- [62] R. X. Silva, H. Reichlova, X. Marti, D. A. B. Barbosa, M. W. Lufaso, B. S. Araujo, A. P. Ayala and C. W. A. Paschoal. *J. Appl. Phys.* **114**, 194102 (2013).
- [63] S. Venugopalan, M. Dutta, A. K. Ramdas, J. P. Remeika, *Phys. Rev. B* **31**, 1490 (1985).